**Amyloid Inhibitors** | Hot Paper

# Multi-Targeting Macrocyclic Peptides as Nanomolar Inhibitors of Self- and Cross-Seeded Amyloid Self-Assembly of α-Synuclein

*Simon Hornung, Dominik P. Vogl, Denise Naltsas, Beatrice Dalla Volta, Markus Ballmann, Beatrice Marcon, Muhammed Muazzam Kamil Syed, Yiyang Wu, Anna Spanopoulou, Regina Feederle, Luzia Heidrich, Jürgen Bernhagen, Thomas Koeglsperger, Günter U. Höglinger, Gerhard Rammes, Hilal A. Lashuel, and Aphrodite Kapurniotu\**

**Abstract:** Amyloid self-assembly of α-synuclein (αSyn) is linked to the pathogenesis of Parkinson's disease (PD). Type 2 diabetes (T2D) has recently emerged as a risk factor for PD. Cross-interactions between their amyloidogenic proteins may act as molecular links. In fact, fibrils of islet amyloid polypeptide (IAPP) (T2D) can cross-seed αSyn amyloidogenesis and αSyn and IAPP colocalize in PD brains. Inhibition of both self- and IAPP-cross-seeded αSyn amyloidogenesis could thus interfere with PD pathogenesis. Here we show that macrocyclic peptides, designed to mimic IAPP self-/cross-interaction sites and previously found to inhibit amyloidogenesis of IAPP and/or Alzheimer's disease (AD) amyloid-β peptide Aβ40(42), are nanomolar inhibitors of both self- and IAPP-cross-seeded amyloid self-assembly of αSyn. Anti-amyloid function is mediated by nanomolar affinity interactions with αSyn via three αSyn regions which are identified as key sites of both αSyn self-assembly and its cross-interactions with IAPP. We also show that the peptides block Aβ42-mediated cross-seeding of αSyn as well. Based on their broad spectrum anti-amyloid function and additional drug-like features, these peptides are leads for multifunctional anti-amyloid drugs in PD, T2D, AD, and their comorbidities, while the identified αSyn key segments are valuable targets for novel, multi-site targeting amyloid inhibitors in PD and related synucleinopathies.

[*] Dr. S. Hornung, Dr. D. P. Vogl, M. Sc. D. Naltsas, Dr. B. D. Volta,
M. Sc. B. Marcon, Dr. A. Spanopoulou, M. Sc. L. Heidrich,
Prof. Dr. A. Kapurniotu
Division of Peptide Biochemistry
TUM School of Life Sciences
Technische Universität München (TUM)
Emil-Erlenmeyer-Forum 5, D-85354 Freising, Germany
E-mail: akapurniotu@tum.de

M. Sc. M. Ballmann, Prof. Dr. G. Rammes
Department of Anesthesiology and Intensive Care
Technische Universität München (TUM)/Klinikum Rechts der Isar
Ismaningerstr. 22, D-81675 Munich, Germany

M. Sc. M. M. K. Syed, Prof. H. A. Lashuel
Laboratory of Molecular and Chemical Biology of Neurodegeneration
École Polytechnique Fédérale de Lausanne (EPFL)
CH 1015 Lausanne, Switzerland

M. Sc. Y. Wu, PD. Dr. T. Koeglsperger, Prof. Dr. G. U. Höglinger
Department of Neurology
LMU University Hospital, Ludwig-Maximilian-University (LMU),
Marchioninistr. 15, D-81377 Munich, Germany
and
German Center for Neurodegenerative Diseases (DZNE)
Feodor-Lynen-Straße 17, D-81377 Munich, Germany
and
Munich Cluster for Systems Neurology (SyNergy)
Feodor-Lynen-Straße 17, D-81377 Munich, Germany

Dr. R. Feederle
Core Facility Monoclonal Antibodies
Helmholtz Center Munich German Research Center
for Environmental Health
Ingolstädter Landstr. 1, D-85764 Neuherberg, Germany
and
Munich Cluster for Systems Neurology (SyNergy)
Feodor-Lynen-Straße 17, D-81377 Munich, Germany
and
German Center for Neurodegenerative Diseases (DZNE) Feodor-Lynen-Straße 17, D-81377 Munich, Germany

Prof. Dr. J. Bernhagen
Division of Vascular Biology
Institute for Stroke and Dementia Research (ISD)
LMU University Hospital, Ludwig-Maximilian-University (LMU)
Feodor-Lynen-Straße 17, D-81377 Munich, Germany
and
Munich Cluster for Systems Neurology (SyNergy)
Feodor-Lynen-Straße 17, D-81377 Munich, Germany

Dr. D. P. Vogl
Current address: Boehringer Ingelheim, Vienna, Austria

Dr. A. Spanopoulou
Current address: ITM Isotope Technologies Munich SE
Garching/Munich, Germany

M. Sc. L. Heidrich
Current address: Life & Brain GmbH, Bonn, Germany

## Introduction

Aberrant amyloid self-assembly is linked to the pathogenesis of more than 50 devastating diseases.[1] These include Parkinson's disease (PD), the second most common neurodegenerative disease after Alzheimer's disease (AD), and type 2 diabetes (T2D), which affect more than 10 and 450 million people worldwide, respectively.

The key amyloid protein in PD is the 140-residue presynaptic protein α-synuclein (αSyn), while the key amyloid polypeptide of T2D is the 37-residue islet amyloid polypeptide (IAPP) (Scheme 1).[1b] In PD brains, large amounts of neurotoxic αSyn oligomers and fibrils are present both in intraneuronal inclusions and extracellularly, mediating inflammation, neurodegeneration, and transmission of pathology.[2] In T2D, IAPP aggregates into cytotoxic oligomers and amyloid fibrils in the pancreas; these assemblies underlie inflammation, β-cell degeneration, and T2D pathogenesis.[3] Under physiological conditions however, IAPP, which is secreted from the pancreatic β-cells and is present both in blood and in brain, functions as a neuroendocrine regulator of glucose homeostasis.[3]

Increasing evidence suggests that T2D is a risk factor for PD.[4] Thereby, cross-interactions between αSyn and IAPP have been suggested to act as a possible molecular link between the two diseases.[5] In fact, in vitro studies showed that IAPP fibrils (fIAPP) are able to act as "cross-seeds", thus strongly accelerating αSyn amyloid self-assembly and these findings were recently confirmed by in vivo studies with PD mouse models.[5a,c] Additional support for a potential pathogenic relevance of αSyn/IAPP cross-interactions for PD includes evidence for αSyn/IAPP co-aggregates in brains of PD patients and for αSyn deposits in the pancreas of PD and T2D patients, and the emerging role of αSyn cross-interactions and cross-seeding events in cell-to-cell spreading of αSyn pathology in PD and related synucleinopathies.[5c,d,6]

Based on the above, devising inhibitors of both self- and fIAPP-cross-seeded amyloid self-assembly of αSyn could be a reasonable approach to suppress PD pathogenesis, in particular also in PD/T2D comorbidity. However, both αSyn and IAPP are intrinsically disordered proteins (IDPs) and cross-interaction sites and structures of their hetero-assemblies are yet unknown, making amyloid inhibitor design a difficult task.[7] In fact, none of the reported αSyn amyloid inhibitors or pipeline PD therapeutics including antibodies, peptides, and small molecules has yet advanced into the clinic or was shown to suppress cross-seeding of αSyn; PD is a still incurable disease.[8]

Macrocyclic peptides are highly attractive drug candidates.[9] The reason is that they can combine, in addition to their own favorable features, key drug-like properties of antibodies and small molecules.[9] Their properties may thus include high potency, high affinity, target selectivity, and the large surface area often required for inhibitors of protein-protein (or IDP/IDP) interactions including anti-amyloid molecules.[9–10] Furthermore, macrocyclic peptides may exhibit, or become engineered to feature, proteolytic stability and BBB permeability, two highly desirable properties for PD anti-amyloid drugs.[9–11]

Previous studies showed that IAPP/amyloid-β peptide (Aβ40(42)) cross-amyloid interaction sites can be used to design peptides as potent inhibitors of their amyloid self-assembly and cross-seeding interactions.[7d,11–12,14] In this context, we have previously designed the IAPP-derived macrocyclic peptides **2b** and **2e** as nanomolar inhibitors of amyloid self-assembly of both IAPP and AD's Aβ40(42) (**2b**) or Aβ40(42)-only (**2e**).[7d,11] The two 17-residue peptides (termed macrocyclic inhibitory peptides or MCIPs) were designed to mimic IAPP surfaces mediating self- and/or cross-interactions with Aβ40(42) while maintaining a minimum amount of recognition elements (Scheme 1).[7d,11] MCIP design was based on the IAPP amyloid core segment IAPP(8–28), containing key recognition elements for both IAPP self-assembly and its cross-interactions with Aβ, and an IAPP(8–28) analog, the linear peptide R3-GI termed IAPP interaction surface mimic (ISM) (Scheme 1).[11–13,15] Importantly, MCIP **2e**, which differs from **2b** only in the presence of D- instead L-amino acids, exhibited high proteolytic stability in human plasma in vitro and BBB-crossing ability in a cell model, making it a lead for AD anti-amyloid drugs.[7d,11]

Here we show that macrocyclic peptides **2b** and **2e** are nanomolar inhibitors of both self- and fIAPP-cross-seeded αSyn amyloid self-assembly. In addition, we show that their
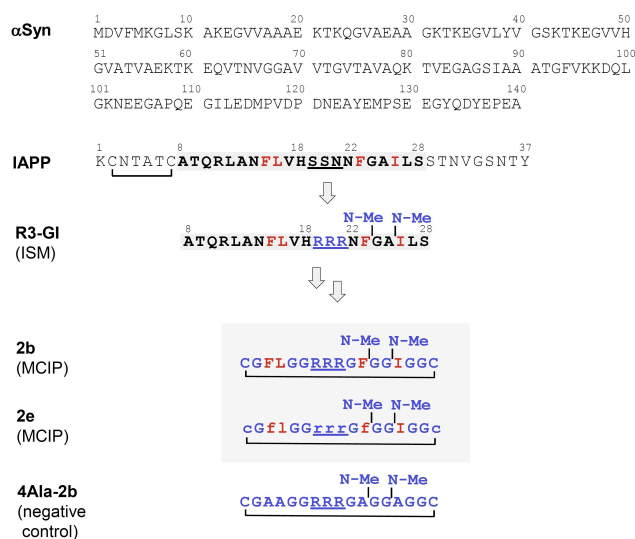


**Scheme 1.** Sequences of αSyn, IAPP, and the previously designed linear template peptide R3-GI (IAPP <u>i</u>nteraction <u>s</u>urface <u>m</u>imic or ISM; IAPP-based sequence numbering), <u>m</u>acrocyclic <u>i</u>nhibitory <u>p</u>eptides (MCIPs) **2e** and **2b**, and negative control peptide **4Ala-2b** (Supporting Tables S1,S2).[11–12] All peptides including IAPP are C-terminal amides.[11–12] IAPP amyloid core IAPP(8–28) is in bold and highlighted in grey; IAPP(19–21), which is replaced by RRR or rrr in IAPP(8–28)-derived peptides, and RRR or rrr segments are underlined (D-amino acids, lower case letters). Colour code: red for the 4 key residues of IAPP self-/cross-interactions with Aβ and blue for non-IAPP residues and amide bond N-methyl groups (N—Me).[11–13] IAPP contains a disulfide bridge between Cys2 and Cys7 and the MCIPs between Cys1 and Cys17.[11]

potent anti-amyloid function is mediated by nanomolar affinity binding to αSyn via 3 αSyn segments which are identified as key sites of both αSyn self-assembly and its cross-interactions with IAPP and that the two peptides also block cross-seeding of αSyn by Aβ42 fibrils (fAβ42).

## Results and Discussion

### *Nanomolar Affinity IAPP/αSyn Cross-Interactions Mediated by IAPP Amyloid Core Region IAPP(8–28)*

We first determined the IAPP regions that mediate its cross-interactions with αSyn. Synthetic peptide arrays containing IAPP decamers covering full-length IAPP and positionally shifted by one residue were incubated with biotin-labeled αSyn (Biotin-αSyn) and Biotin-αSyn-bound decamers were visualized by chemiluminescence.[15a] We found a major cluster of 4 consecutive decamers within IAPP(8–20), while a second weaker cluster localized in IAPP(13–27) (Figure 1a, Supporting Figure S1). We then titrated synthetic Nα-terminal fluorescein-labeled IAPP (Fluos-IAPP) and IAPP(8–28) (Fluos-IAPP(8–28)) with αSyn. This method capitalizes on the dependence of the fluorescence emission of a fluorophore on its local environment and its change upon ligand binding which correlates with the extent of complex formation.[16] Binding of αSyn to the labeled peptides resulted in an αSyn concentration-dependent fluorescence enhancement (Figure 1b, c). This enhancement could be due to the increased rigidity of the fluorophore in the hetero-complex. Sigmoidal titration curves were obtained and yielded low nanomolar apparent (app.) $K_d$ values of 26.7 ($\pm$6.0) nM for the Fluos-IAPP/αSyn interaction and 8.2 ($\pm$2.3) nM for the Fluos-IAPP(8–28)/αSyn interaction (means ($\pm$SD), 3 assays) (Figure 1b, c). This data revealed that IAPP binds αSyn with low nanomolar affinity and that the IAPP amyloid core IAPP(8–28) contains the key recognition elements for the IAPP/αSyn interaction as earlier found for the IAPP/IAPP and the IAPP/Aβ40(42) interactions.[13,15a]
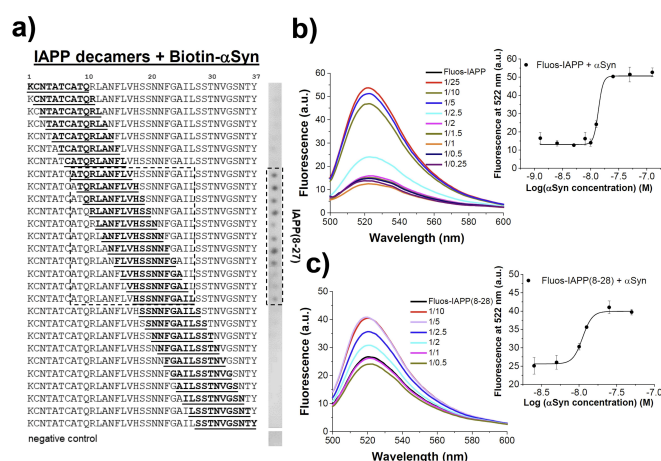


**Figure 1.** Identification of IAPP regions that interact with αSyn by using peptide arrays (a) and determination of the binding affinities of interactions of αSyn with IAPP and IAPP(8–28) by fluorescence spectroscopic titrations (b,c). a) Synthetic peptide arrays containing IAPP decamers (bold & underlined) were incubated with Biotin-αSyn (0.5 μM); decamers which bound Biotin-αSyn are in dashed rectangles. Array representative of two arrays synthesized in parallel and two independent incubations with Biotin-αSyn. b,c) Fluorescence emission spectra of Fluos-IAPP (b) and Fluos-IAPP(8–28) (c) (5 nM) alone or their mixtures with various molar ratios of αSyn (Fluos-peptide/αSyn) as indicated; data from 1 representative assay out of 3. Insets show binding curves; data means ($\pm$SD) of 3 titration assays.

### *Macrocyclic Peptides 2 b and 2 e are Nanomolar Inhibitors of Self- and IAPP-Cross-Seeded Amyloid Self-Assembly of αSyn*

Based on the above, we hypothesized that the IAPP(8–28)-derived macrocyclic peptides **2b** and **2e** might mimic IAPP/αSyn cross-interaction surfaces and interfere with αSyn amyloid self-assembly and its cross-seeding by fIAPP. Notably, initial studies showed that both IAPP(8–28), which is intrinsically amyloidogenic, and its non-amyloidogenic analogs IAPP(8–28)-GI and R3-GI, two linear MCIP precursors, were unable to inhibit αSyn fibrillogenesis (Scheme 1, Supporting Table S1, Supporting Figure S2).[11–12,17]

The effects of **2b** and **2e** on αSyn amyloid self-assembly were then studied (Scheme 1, Figure 2a–c, Table 1). In parallel, we studied the effects of the negative control peptide **4Ala-2b** in which all four IAPP-derived key residues of **2b** and **2e** were replaced by Ala (Scheme 1).[11] According to the amyloid specific Thioflavin T (ThT) binding assay and transmission electron microscopy (TEM), αSyn fibrillogenesis started after a lag-time of ~24 h and was apparently completed at ~48 h (Figure 2a, b & Supporting Figure S3a-c). However, in the presence of **2b** or **2e** (αSyn/peptide 1/1) a full suppression of αSyn fibrillogenesis was observed (Figures 2a, b & Supporting Figure S3b,c). In addition, **2b** and **2e** strongly suppressed

**Table 1:** IC$_{50}$ of inhibitory effects of **2b**, **2e**, and **4Ala-2b** on cell-damaging effects of un-seeded, fαSyn-seeded, and fIAPP-cross-seeded αSyn amyloid self-assembly.

| Peptide | IC$_{50}$ ($\pm$SD) (nM) Inhibition of αSyn[a] | IC$_{50}$ ($\pm$SD) (nM) Inhibition of αSyn + fαSyn[a] | IC$_{50}$ ($\pm$SD) (nM) Inhibition of αSyn + fIAPP[a] |
|---|---|---|---|
| **2b** | 62.3 ($\pm$33.9) | 51.8 ($\pm$4.8) | 75.2 ($\pm$21.1) |
| **2e** | 66.0 ($\pm$23.3) | 54.7 ($\pm$4.4) | 42.0 ($\pm$18.5) |
| **4Ala-2b** | >5000 | >5000 | >5000 |

[a] IC$_{50}$ values, means ($\pm$SD) from 3 titration assays ($n=3$ wells each); αSyn, 100 nM w/o or with preformed fαSyn or fIAPP seeds (10%).
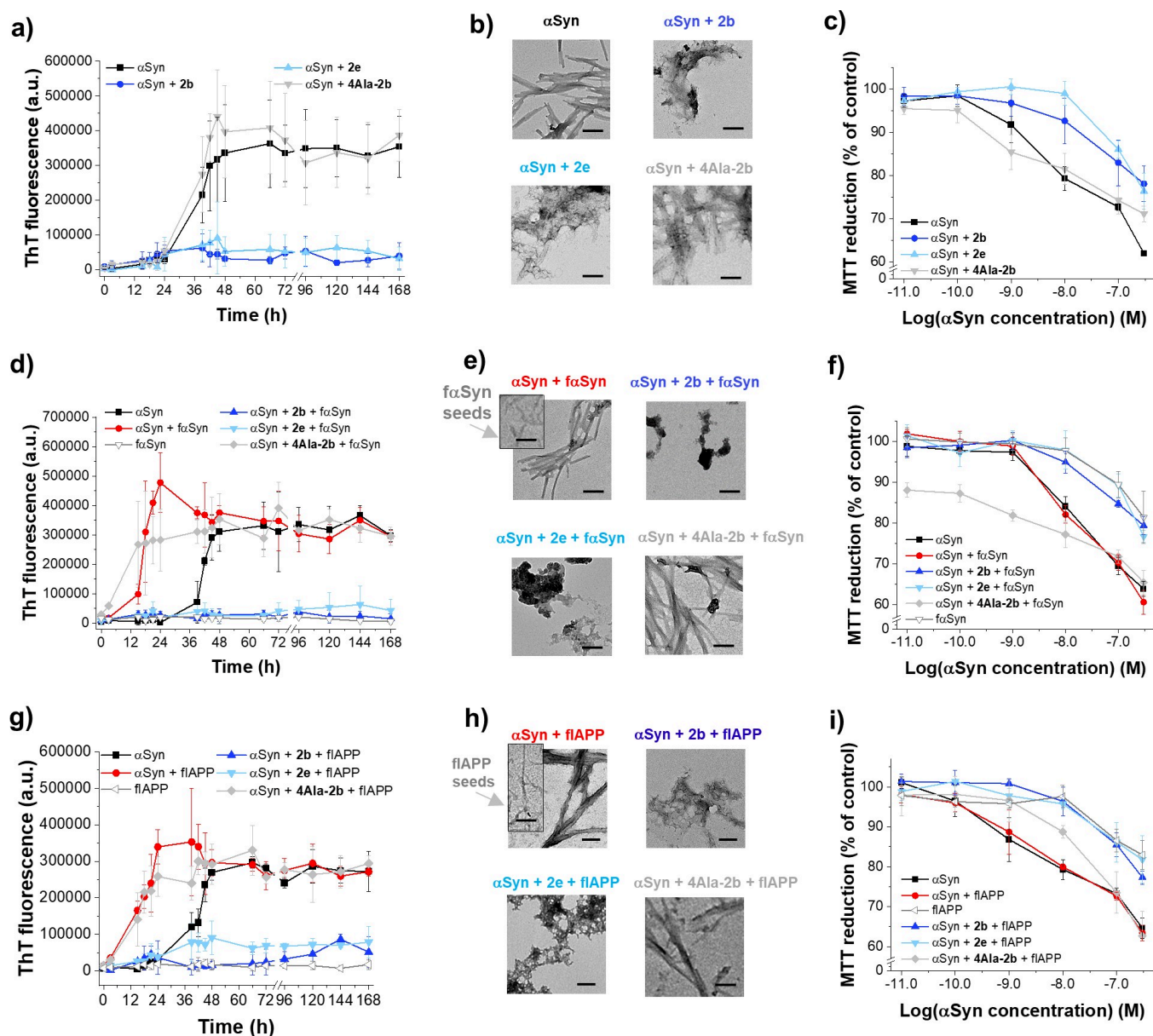
**Figure 2.** Effects of **2b**, **2e**, and **4Ala-2b** on non-seeded (a–c), seeded with preformed fαSyn (d–f), and flAPP-cross-seeded αSyn amyloid self-assembly and related cell-damaging effects (g–i). a–c) Fibrillogenesis of αSyn (3 μM) alone or in the presence of **2b** and **2e** (1/1) or **4Ala-2b** (1/50) determined by ThT binding (means (±SD), 3 assays (3 wells each)) (a); TEM images of solutions (7 day-aged) from (a) as indicated (color code as in (a)) (scale bars, 100 nm) (b); PC12 cell viability after treatment with solutions from (a) (7 day-aged) determined by the MTT reduction assay (means (±SD), 3 assays (3 wells each)) (c). d–f) Fibril formation of αSyn alone (3 μM) or seeded by preformed fαSyn (10%) alone or with **2b** and **2e** (1/1) or **4Ala-2b** (1/50) as determined by the ThT binding assay and ThT binding of fαSyn seeds (0.3 μM) (means (±SD), 3 assays (3 wells each)) (d); TEM images of solutions from (d) aged for 7 days (seeded αSyn/**2b**(**2e**) mixtures) or for 24 h (seeded αSyn alone or with **4Ala-2b**) and from fαSyn seeds (scale bars, 100 nm) (e); PC12 cell viability after treatment solutions from (d) (7 day-aged) determined by the MTT reduction assay (means (±SD), 3 assays (3 wells each)) (f). g-i) Fibrillogenesis of αSyn (3 μM) alone or cross-seeded by flAPP (10%) alone or with **2b** and **2e** (1/1) or **4Ala-2b** (1/50) determined by ThT binding and ThT binding of flAPP seeds (0.3 μM) (means (±SD), 3 assays (3 wells each)) (g); TEM images of solutions from (g) aged for 7 days (cross-seeded αSyn/**2b**(**2e**)) or for 24 hours (cross-seeded αSyn alone or with **4Ala-2b**) as indicated (scale bars, 100 nm) (h); PC12 cell viability after treatment with solutions from (g) (7 day-aged) determined by the MTT reduction assay (means (±SD), 3 assays (3 wells each)) (i).

formation of cell-damaging αSyn assemblies according to the 3-[4,5-dimethylthiazol-2-yl]-2,5-diphenyltetrazolium bromide (MTT) reduction assay in cultured rat pheochromocytoma (PC12) cells (Figure 2c, Supporting Figure S3d,e). In fact, αSyn titrations with **2b** and **2e** revealed

nanomolar IC$_{50}$ values, i.e. 62.3 (±33.9) nM (**2b**) and 66.0 (±23.3) nM (**2e**) (Table 1, Supporting Figure S3d,e). No attenuating effects were found for the negative control **4Ala-2b** up to a 50-fold higher molar excess than **2b** or **2e** (Figure 2a–c).

We next asked whether **2b** and **2e** might also suppress seeding of αSyn fibrillogenesis by preformed αSyn fibrils (fαSyn). Addition of fαSyn seeds (10%) to αSyn strongly accelerated formation of αSyn fibrils and cell-damaging aggregates as expected (Figure 2d–f, Supporting Figure S4). However, in the presence of **2b** and **2e** (1/1), αSyn fibrillogenesis and cell toxicity were fully suppressed whereas again **4Ala-2b** (αSyn/**4Ala-2b**, 1/50) did not inhibit (Figure 2d–f, Supporting Figure S4). Titrations with the two inhibitors yielded IC$_{50}$ values of 51.8 ($\pm$4.8) nM (**2b**) and 54.7 ($\pm$4.4) nM (**2e**) which were nearly identical to the IC$_{50}$ values of effects on unseeded αSyn fibrillogenesis (Table 1, Supporting Figure S5). Notably, **2b** and **2e** inhibited αSyn fibrillogenesis and cytotoxicity when seeding was performed both with 10% and 1% fαSyn seeds, indicative of effects on secondary nucleation and fibril elongation events (Figure 2d–f, Supporting Figure S4–S6).[18]

We then asked whether the two peptides might also interfere with the cross-seeding effect of IAPP fibrils (fIAPP) on αSyn fibrillogenesis.[5a] Addition of seed amounts (10%) of preformed IAPP fibrils (fIAPP) to αSyn strongly accelerated its fibrillogenesis consistent with previous findings (Figure 2g, h).[5a] In parallel, a strong acceleration of formation of cell-damaging αSyn species was also observed (Supporting Figure S7a,b). Importantly, in the presence of **2b** or **2e** (1/1) a full suppression of cross-seeding of αSyn fibrillogenesis and cytotoxicity was found and titrations yielded nanomolar IC$_{50}$ values for both peptides, i.e. 75.2 ($\pm$21.1) nM (**2b**) and 42.0 ($\pm$18.5) nM (**2e**) (Table 1, Supporting Figure S7c-h). As expected, **4Ala-2b** (50-fold) did not inhibit (Figure 2g–i). Notably, **2b** and **2e** were non-amyloidogenic and non-cytotoxic up to at least 200-fold higher concentrations than the IC$_{50}$ values consistent with the design concept and previous results (Supporting Figure S8).[11–12,19]

Taken together, the above studies identified MCIPs **2b** and **2e** as nanomolar inhibitors of both self- and fIAPP-cross-seeded amyloid self-assembly of αSyn.

### MCIPs Bind αSyn with Nanomolar Affinity and Sequester it into Non-Fibrillar and Non-Cytotoxic Co-Assemblies

To learn more about the inhibition mechanism, αSyn/peptide interactions and co-assemblies were studied by various biophysical and biochemical methods. First, the affinities of αSyn/peptide interactions were determined by fluorescence spectroscopic titrations of synthetic N-terminal fluorescein-labeled **2b** (Fluos-**2b**) and **2e** (Fluos-**2e**) with αSyn (Figure 3a, b). Low nanomolar app. K$_d$ values were obtained for both interactions (Fluos-**2b**/αSyn, app. K$_d$=17.2 ($\pm$2.6) nM; Fluos-**2e**/αSyn app. K$_d$=22.0 ($\pm$5.1) nM) in good agreement with the IC$_{50}$ values (Figure 3a, b, Tables 2 & 1). Of note, **2b** and **2e** were mostly monomeric at low nanomolar concentrations but self-assembled into soluble oligomers at higher concentrations as expected from their design concept and previous findings (Supporting Figure S9).[11–12,20] Also, their αSyn binding affinities were very similar to their IAPP binding affinities while **4Ala-2b** did not bind either IAPP or αSyn (Supporting Figure S10, S11, Table 2)).[11]

The far-UV CD spectrum of freshly dissolved αSyn exhibited a pronounced minimum at ~200 nm indicative of mainly disordered structure consistent with previous reports (Figure 3c, d).[21] Following aging for 48 h, a marked reduction of the CD magnitude was observed indicative of αSyn oligomerization.[21a,b] In the presence of **2b** or **2e**, however, no/slower reduction of the CD magnitude was observed in line with their inhibitory activity on αSyn amyloid self-assembly (Figure 3c, d). Also, in addition to the minimum at ~200 nm, the CD spectra of αSyn/inhibitor mixtures exhibited a weaker but clear minimum between 220–230 nm. Their shapes and magnitudes suggested that hetero-complexes were more ordered than αSyn (Figure 3c, d).

Next, αSyn/inhibitor hetero-complexes were cross-linked with glutaraldehyde and following separation by SDS-PAGE visualized by western blot (WB) with anti-αSyn and anti-**2e**(**2b**) antibodies (Figure 3e & Supporting Figure S12). In freshly made αSyn solutions, monomers and dimers were major species; trimers and other medium-to-high MW aggregates tended to be less abundant.[21c] In αSyn/**2b**(**2e**) mixtures, a similar pattern as in αSyn alone was observed with the difference that the bands stained with both the anti-αSyn and a monoclonal anti-**2e**(**2b**)

**Table 2:** App. K$_d$s of interactions of Fluos-**2b**, -**2e**, and -IAPP with IAPP, αSyn, and the three identified αSyn key segments determined by fluorescence spectroscopic titrations.[a]

| Binding partner | App. K$_d$ ($\pm$SD) (nM) (**2b**) | App. K$_d$ ($\pm$SD) (nM) (**2e**) | AApp. K$_d$ ($\pm$SD) (nM) (IAPP) |
|---|---|---|---|
| IAPP | 29.6 ($\pm$19.3) | 46.9 ($\pm$33.4) | 9.7 ($\pm$0.9)[19] |
| αSyn | 17.2 ($\pm$2.6) | 22.0 ($\pm$5.1) | 26.7 ($\pm$6.0) |
| αSyn(1–14) | 366.2 ($\pm$115.8) | 461.3 ($\pm$47.5) | 886.4 ($\pm$552.0) |
| αSyn(34–52) | 662.8 ($\pm$9.4) | 504.7 ($\pm$171.2) | 347.5 ($\pm$103.2) |
| αSyn(87–105) | 72.1 ($\pm$20.5) | 122.2 ($\pm$17.1) | 31.9 ($\pm$0.6) |

[a] App. K$_d$s, means ($\pm$SD) from 3 binding curves (3 titration assays) using N$^\alpha$-terminal fluorescein-labeled **2b** (Fluos-**2b**), **2e** (Fluos-**2e**), and IAPP (Fluos-IAPP) (pH 7.4). Fluos-peptides 5 nM except for titrations of Fluos-**2b**(**2e**) with αSyn and of Fluos-IAPP with IAPP (data from ref. [19]) (Fluos-peptides 1 nM).[19]
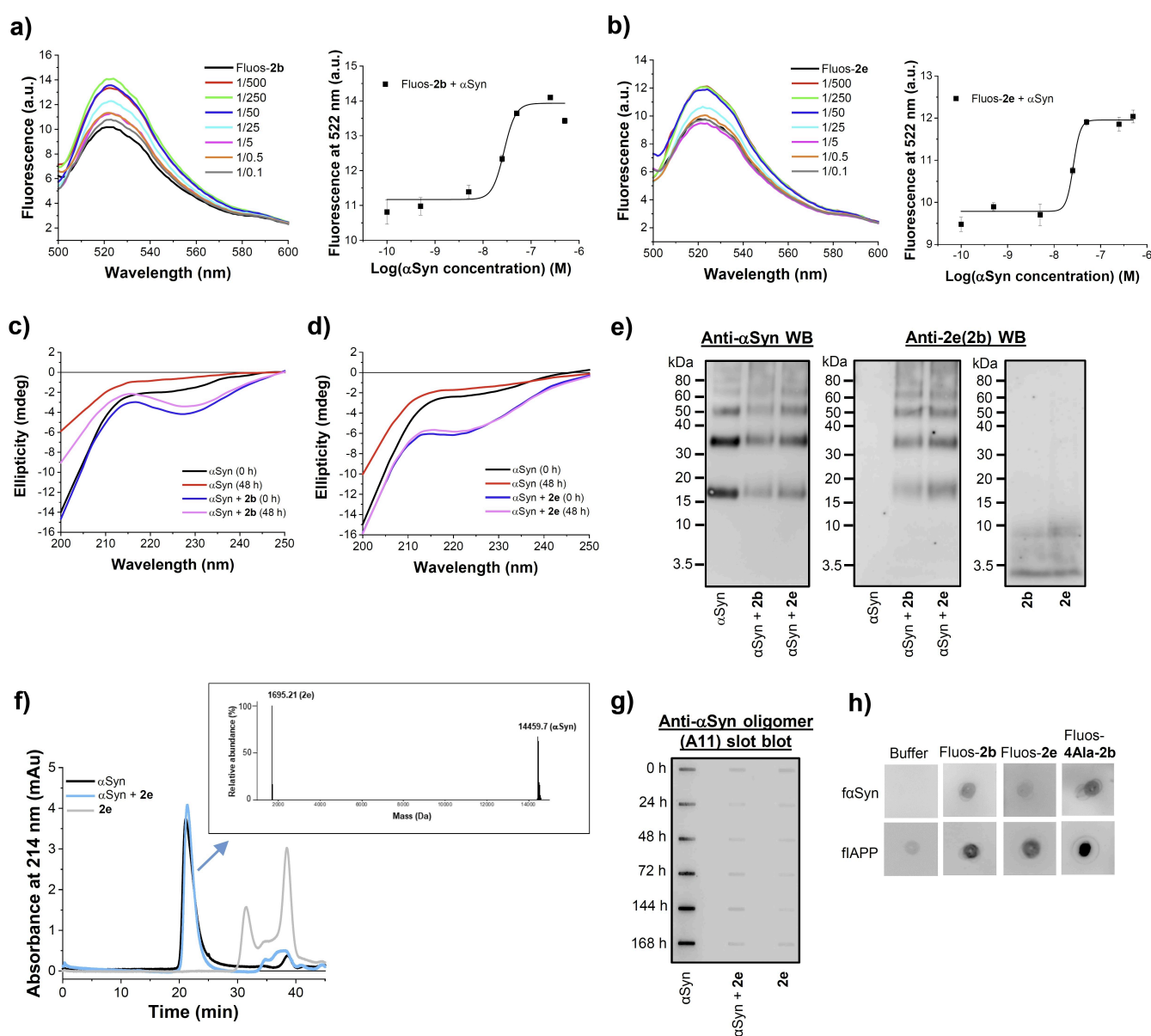
**Figure 3.** Studies on interactions, hetero-complexes, and mechanism of inhibitory effects of **2e** and **2b** on αSyn amyloid self-assembly. a,b) Left, app. $K_d$s of interactions of Fluos-**2b** (a) and Fluos-**2e** (b) with αSyn determined by fluorescence spectroscopic titrations. Fluorescence emission spectra of Fluos-**2b** or Fluos-**2e** (1 nM) and their mixtures with various molar ratios of αSyn are shown as indicated; spectra from 1 representative binding assay out of 3. Right side, binding curves; data means ($\pm$SD) of 3 titration assays; app. $K_d$s in Table 2. c, d) Far-UV CD spectra of αSyn (1 μM) alone and its mixtures with **2b** (c) or **2e** (d) (10 μM) measured at 0 h and after 48 h of incubation. e) Characterization of αSyn/MCIP hetero- and αSyn homo-oligomers by cross-linking with glutaraldehyde, SDS-PAGE, and western blot with anti-αSyn (left) or anti-**2e**(**2b**) (right) antibodies (αSyn, 10 μM; MCIPs, 50 μM) antibody (see also Supporting Figure S12); representative results from 3 assays. f) Characterization of αSyn/**2e** hetero-complexes in comparison to αSyn and **2e** alone by size exclusion chromatography (SEC). Chromatograms of αSyn (3 μM), **2e** (30 μM), and the αSyn/**2e** mixture (1/10) are shown. Inset, ESI-MS spectrum (deconvoluted) of the 21 min peak from SEC of the αSyn/**2e** mixture (see also Supporting Figure S14). Determined MWs as indicated; calculated mass (average) 14460.27 Da (αSyn) and 1695.04 Da (**2e**). Representative results from 3 SEC analyses and ESI-MS. g) Kinetics of αSyn self-assembly into A11-reactive toxic oligomers alone or in the presence of **2e** followed by slot blot analysis using the A11 antibody (see also Supporting Figure S15). Solutions αSyn (3 μM) alone, αSyn/**2e** (1/1), and **2e** (3 μM) alone were analyzed at indicated incubation time points. Representative results from 4 assays. h) Binding of **2b**, **2e**, and **4Ala-2b** to fαSyn and fIAPP determined by dot blot analysis. Fluos-**2b**, Fluos-**2e**, and Fluos-**4Ala-2b** (1.5 μM) and the buffer alone control were incubated with membranes containing spotted fαSyn or fIAPP; binding was visualized by fluorescence (see also Supporting Figure S16). Representative results from 3 assays.

antibody; in addition, bands corresponding to αSyn mono-, di-, and trimers were slightly shifted upwards. This data indicated that **2b** and **2e** co-assemble with αSyn monomers and low MW oligomers into hetero-dimers and low MW hetero-oligomers.

Hetero-complexes formed at early steps of αSyn/**2e** co-assembly were then studied by size exclusion chromatography (SEC) (Figure 3f). αSyn monomers (~15 kDa) present in freshly made αSyn alone solutions eluted at a retention time ($t_R$) of ~21 min corresponding to a globular protein of ~44 kDa; this was due to its natively unfolded nature resulting in a higher hydrodynamic radius (Figure 3f, Supporting Figure S13).[21a,b] In **2e** alone (~2 kDa) solutions, the major fraction eluted at ~38 min and corresponded to **2e** monomers while a smaller fraction corresponding to **2e** oligomers eluted at ~32 min. Importantly, in the αSyn/**2e** mixtures, the 21 min peak found in αSyn alone was still present but the **2e** alone peaks were strongly diminished (Figure 3f). These findings were consistent with formation of αSyn/**2e** hetero-complexes which eluted at ~21 min and were confirmed by electrospray ionization mass spectrometry (ESI-MS) (Figure 3f, Supporting Figure S14). The observed lack of a shift of the αSyn peak to higher MWs in the αSyn/**2e** mixture was most likely due to the low MW of **2e** and the resolution limit of the column. Together, the above studies suggested αSyn/**2e** hetero-dimers and low MW hetero-oligomers as early species in the αSyn/**2e** co-assembly pathway.

Formation of cytotoxic αSyn oligomers is associated with neurodegeneration and PD pathogenesis.[22] Our ThT binding and MTT reduction assays suggested that in the presence of the MCIPs formation of cytotoxic assemblies of αSyn was strongly suppressed (Figure 2a–c). To characterize the effects of MCIPs on formation of αSyn oligomers more directly, we followed kinetics of cytotoxic oligomer formation in αSyn alone and its mixtures with **2e**. We used slot blot analysis and the antibody A11 reported to recognize toxic oligomers of various different proteins including αSyn (Figure 3g, Supporting Figure S15a).[23] Formation of cytotoxic αSyn oligomers was further confirmed by MTT reduction and TEM (Supporting Figure S15b–e). In αSyn alone, good amounts of cytotoxic A11-reactive oligomers were present in ~48 h-aged solutions (Figure 3g, Supporting Figure S15). By contrast, significantly lower amounts of A11-reactive oligomers and no cytotoxic effects were observed in the αSyn/**2e** mixtures (1/1) (Figure 3g, Supporting Figure S15a, b).

The potent inhibitory activity of the MCIPs could also be mediated by binding to fαSyn and/or fIAPP resulting in suppression of secondary nucleation and/or fibril elongation.[18] In fact, dot blot assays showed that Fluos-**2b** and Fluos-**2e** are able to bind both fαSyn and fIAPP (Figure 3h). However, the non-inhibitor Fluos-**4Ala-2b** also bound -most likely non-specifically-(Figure 3h, Supporting Figure S16). In addition, sub-stoichiometric amounts of **2b** and **2e** did not markedly affect self-/cross-seeded αSyn fibrillogenesis (Supporting Figure S3, S5, S7). Furthermore, αSyn/**2e**(**2b**) hetero-complexes were unable to become (cross−)seeded by fαSyn or fIAPP consistent with a key role in MCIPs' anti-amyloid function (Supporting Figure S17, S18).

In conclusion, the anti-amyloid effects of **2b** and **2e** on αSyn are likely mediated by high affinity interactions between monomeric and/or oligomeric states of MCIPs and αSyn resulting in αSyn sequestration into amorphous, non-cytotoxic, and non-(cross−)seedable αSyn/MCIP co-assemblies. Interestingly, a similar mechanism has been suggested to underlie inhibitory effects of MCIPs and related IAPP-derived inhibitors on amyloid self-assembly of IAPP and Aβ40(42).[11–12,14a,20]

### Additional Anti-Amyloid Effects of the MCIPs

The impairment of hippocampal synaptic long term potentiation (LTP) by αSyn oligomers is believed to be directly linked to neuronal dysfunction in PD.[2a,24] To obtain first information about the potential physiological relevance of our in vitro findings, we investigated the effects of the two MCIPs on αSyn oligomer-mediated impairment of hippocampal synaptic LTP in mouse brains ex vivo (Figure 4a–c). In fact, electrophysiological studies showed that synaptic LTP damage caused by preformed cytotoxic αSyn oligomers was significantly reduced by **2b** or **2e** (Figure 4a–c, Supporting Figure S19).[24a] Effects of the MCIPs on αSyn toxicity were also studied using αSyn overexpressing postmitotic dopaminergic Lund human mesencephalic (LUHMES) neurons, a previously developed disease-relevant cell model for the screening of putative modulators of αSyn toxicity.[25] αSyn cytotoxicity was quantified by the lactate dehydrogenase (LDH) release assay. Importantly, significant protection of the neurons was found for both peptides providing additional support for their anti-amyloid function (Figure 4d). In addition, as Aβ-mediated cross-seeding of αSyn may play a role in AD/PD co-pathology we asked whether **2b** and **2e**, found to also inhibit Aβ amyloid self-assembly, may affect this process as well.[26] In fact, ThT binding, TEM, and cell viability studies revealed a full suppression of fAβ42-cross-seeding of αSyn in their presence (1/1) (Figure 4e–g). Finally, ThT binding studies showed that **2b** and **2e** do not inhibit insulin fibrillogenesis although their precursors IAPP and IAPP-GI were found to inhibit this process (Supporting Figure S20).[14c] Since **2b** inhibits amyloid self-assembly of Aβ40(42), IAPP, and αSyn whereas **2e** inhibits Aβ40(42) and αSyn but not IAPP, our findings support the notion that the anti-amyloid multifunctionality of the two peptides is target-selective.[11] Studies with additional putative interaction partners will be required to further address this issue.

### Three αSyn Key Regions Mediate its High Affinity Interactions with both the MCIPs and IAPP: Multi-Site Binding Underlies MCIP Anti-Amyloid Function

To identify αSyn regions mediating its high affinity interactions with MCIPs, we incubated synthetic peptide arrays containing αSyn decamers covering its entire sequence and positionally shifted by one residue with Fluos-**2e** (Figure 5a, Supporting Figure S21).

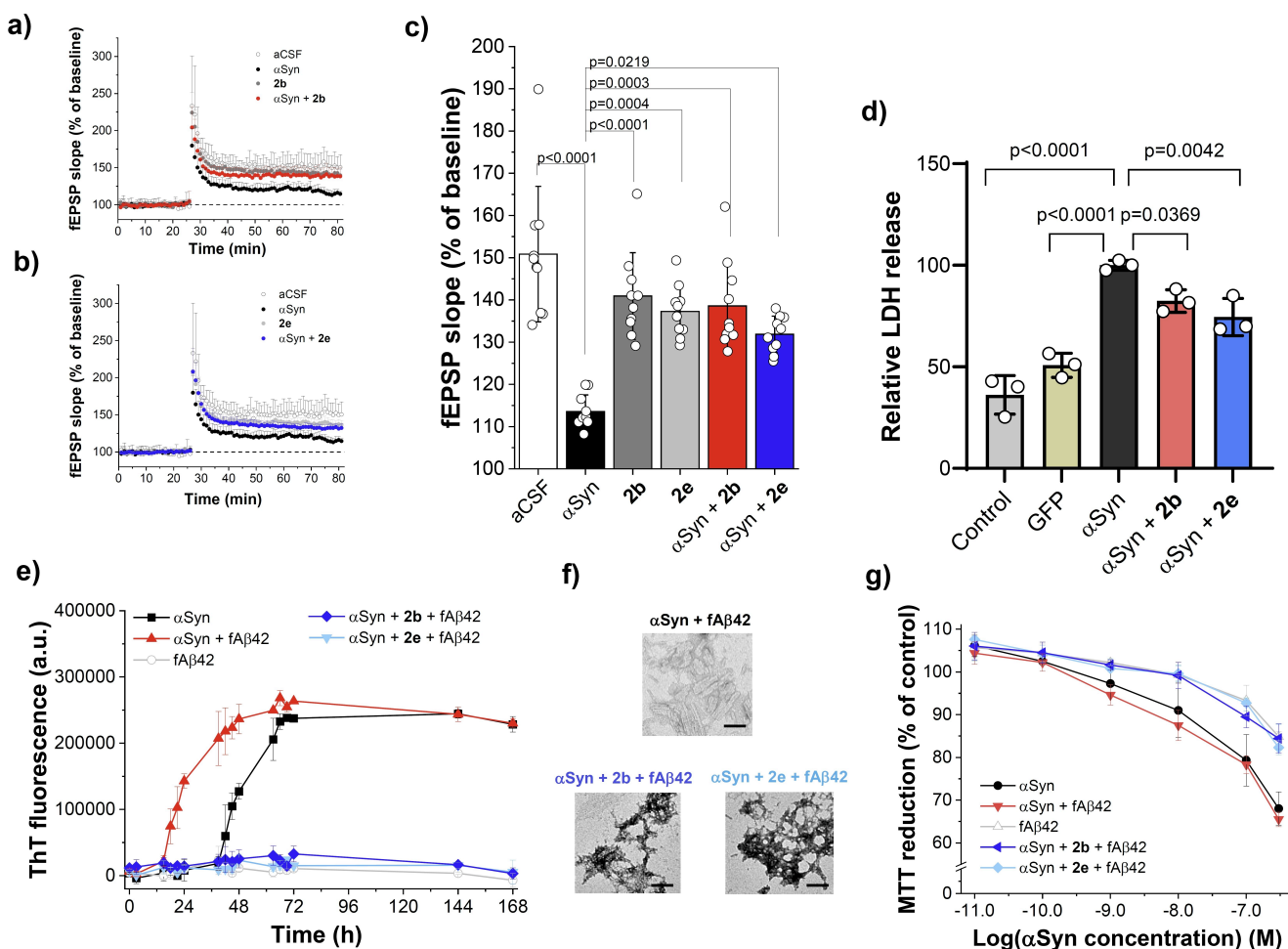We identified 3 clusters of strong binding decamers: one localized within the N-terminal segment αSyn(1–14), a

**Figure 4.** MCIPs ameliorate αSyn-mediated synaptic damage in mouse brains ex vivo (a–c), suppress αSyn cytotoxicity in αSyn overexpressing human postmitotic dopaminergic neurons (d), and block cross-seeding of αSyn amyloid self-assembly by Aβ42 fibrils (fAβ42) (e–g). a–c) Suppression of αSyn oligomer-induced LTP impairment in murine hippocampal slices ex vivo by **2b** and **2e**. a, b) Time course of synaptic transmission (fEPSP, field excitatory postsynaptic potential) after treatment with artificial cerebrospinal fluid (aCSF) medium (buffer control), αSyn oligomers (175 nM), **2b** (a) or **2e** (b) alone (1.75 µM), and αSyn oligomers/**2b** (a) or **2e** (b) mixture (1/10) as indicated; data means ($\pm$SD), from $n=10$ samples/treatments each. c) LTP values: bars show the averages from the last 10 min of recording; data means ($\pm$SD), $n=10$ for each group; p-values as indicated; calculated using non-parametric testing with Mann-Whitney U-tests or a Kruskal-Wallis test. (d) Suppression of αSyn-mediated toxicity in αSyn overexpressing human postmitotic dopaminergic LUHMES neurons by by **2b** and **2e** (10 nM) measured by LDH release. Grey column (control): untransduced cells; dark yellow column (GFP): cells transduced with GFP (control for virus); black column (αSyn): αSyn overexpressing cells without treatment; red column (αSyn+**2b**): αSyn overexpressing cells treated with **2b**; blue column (αSyn+**2e**): αSyn overexpressing cells treated with **2e**. Data means ($\pm$SEM) from 3 assays ($n=3$ each). Statistical significance was determined using one-way ANOVA, followed by Dunnett's multiple comparisons test; p-values as indicated. e-g) MCIPs block cross-seeding of αSyn amyloid self-assembly by fAβ42. Fibrillogenesis of αSyn (3 µM) alone or cross-seeded by fAβ42 (20%) alone or with **2b** and **2e** (1/1) determined by ThT binding; data of fAβ42 seeds (0.6 µM) is also shown for comparison; data means ($\pm$SD), 3 assays (3 wells each) (e); TEM images of 7 day-aged solutions from (e) (scale bars, 100 nm) (f); PC12 cell viability after treatment with 7 day-aged solutions from (e) determined by the MTT reduction assay (means ($\pm$SD), 3 assays (3 wells each)) (g). P values < 0.05 were considered significant.

2nd one within αSyn(34–52), and a 3rd one within αSyn(87–105) (Figure 5a, Supporting Figure S21). The results of the peptide array studies were confirmed and quantified by fluorescence spectroscopic titrations which revealed nanomolar app. $K_d$s for the interactions of **2e** and **2b** with all 3 αSyn segments (Figure 5b–d, Supporting Figure S22, Table 2). This data showed that the high affinity binding of MCIPs to αSyn is mediated via the 3 αSyn regions αSyn(1–14), αSyn(34–52), and αSyn(87–105).

Because MCIPs might mimic IAPP sites mediating its cross-interactions with αSyn, we hypothesized that they might interact with the same/similar αSyn regions as IAPP which could underlie their potent inhibitory activity on IAPP-mediated cross-seeding. To address this, the αSyn peptide array was incubated with Fluos-IAPP. We identified 3 major binding clusters corresponding to αSyn(1–13), αSyn(34–46), and αSyn(87–104) and a weaker one within the NAC region corresponding to αSyn(68–80) (Figure 5e, Supporting Figure S23). Importantly, the 3 major IAPP-
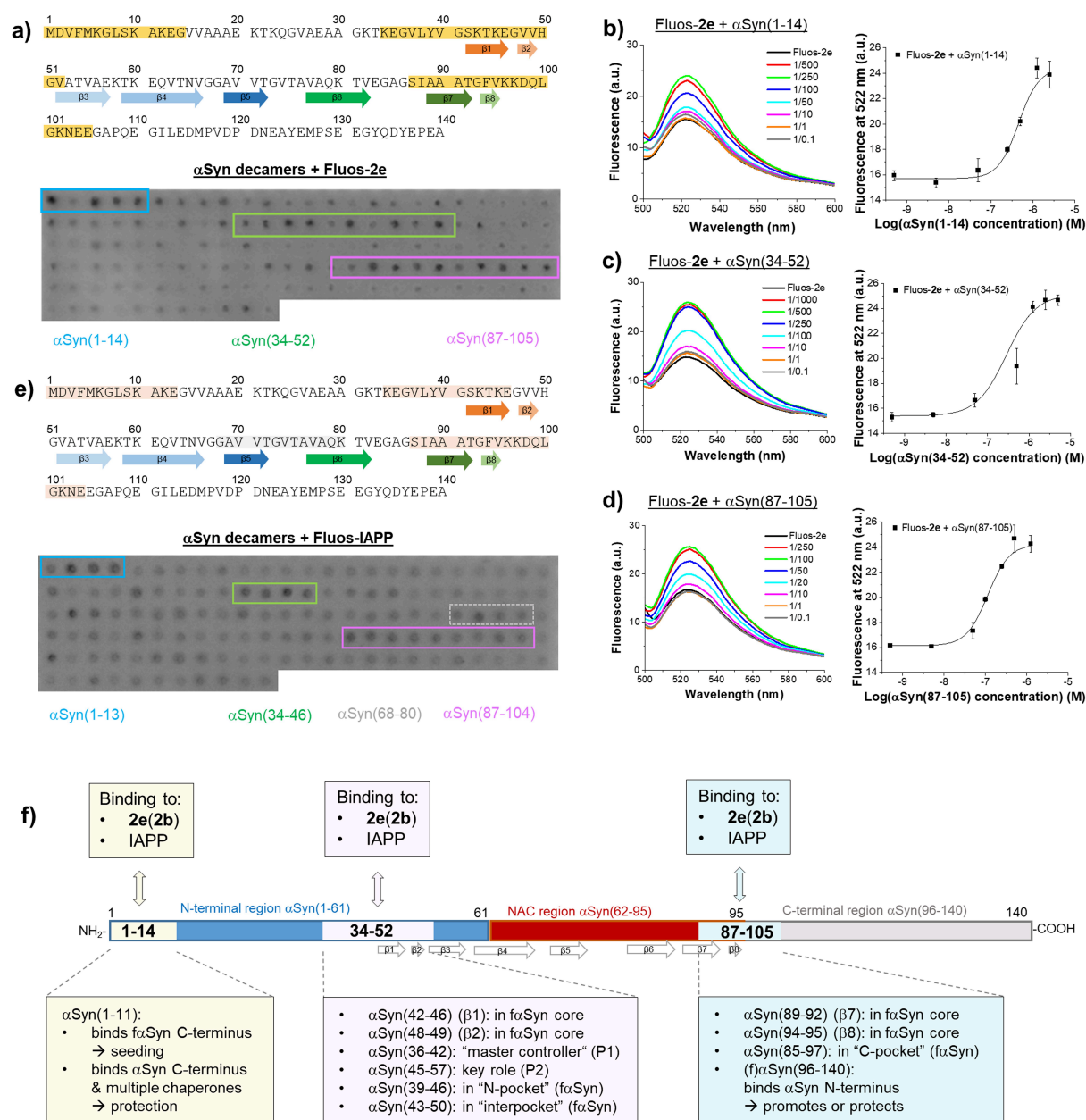
**Figure 5.** Identification of αSyn segments mediating its interactions with MCIPs and IAPP by synthetic peptide arrays (a, e), determination of binding affinities by fluorescence spectroscopic titrations (b–d), and overview of key αSyn interaction sites and related functions (f). a) Identification of key αSyn regions interacting with **2e** using peptide arrays. Top, αSyn sequence; identified **2e**-binding regions in orange rectangles as indicated; colored arrows indicate β-strands β1-β8 in the fαSyn fold of Guerreiro-Ferreira et al.[27] Bottom, peptide array containing αSyn decamers following incubation with Fluos-**2e** (1 μM) and bound peptide visualization by fluorescence; identified Fluos-**2e**-binding segments αSyn(1–14), αSyn(34–52), and αSyn(87–105) in coloured rectangles. Array representative of 2 arrays synthesized in parallel and 2 independent incubations with Fluos-**2e** (Supporting Figure S21). b–d) Determination of app. $K_d$s of Fluos-**2e** interactions with identified **2e**-binding αSyn segments by fluorescence spectroscopic titrations. Left, fluorescence emission spectra of Fluos-**2e** alone (5 nM) or with various molar ratios of αSyn(1–14) (b), αSyn(34–52) (c), and αSyn(87–105) (d) (Fluos-**2e**/peptide as indicated). Spectra from 1 representative assay out of 3. Right, binding curves; data means (±SD) of 3 assays (see Table 2). e) Identification of key αSyn regions interacting with IAPP using peptide arrays. Top, αSyn sequence; IAPP-binding regions highlighted in pink (major) or grey (weaker); colored arrows as under (a).[27] Bottom, peptide array containing αSyn decamers (as in (a)) following incubation with Fluos-IAPP (1 μM) and visualization. Identified 3 major Fluos-IAPP-binding segments αSyn(1–13), αSyn(34–46), and αSyn(87–104) in coloured rectangles (made by solid lines); weaker binding αSyn(68–80): rectangle made by dashed lines. Array representative of two arrays synthesized in parallel and two independent incubations with Fluos-IAPP (Supporting Figure S23). f) Schematic overview of the 3 identified key αSyn segments mediating its interactions with **2e**, **2b**, and IAPP and previously reported interactions & functions of related αSyn sequence parts.[23b,27–28] White arrows indicate β-strands β1-β8 in the fαSyn fold of Guerreiro-Ferreira et al.[27]

binding αSyn regions were nearly identical to the MCIP-binding ones which was consistent with our hypothesis. Furthermore, fluorescence spectroscopic titrations confirmed that the 3 major MCIP-binding αSyn segments bind (f)IAPP as well and revealed that the affinities of their interactions with IAPP were very similar to the affinities of their interactions with **2b** and **2e** (Supporting Figure S24, S25, Table 2). Together, the above studies identified segments αSyn(1–14), αSyn(34–52), and αSyn(87–105) as key sites of the high affinity interactions of αSyn with both the MCIPs and IAPP.

Remarkably, the identified αSyn segments mediating interactions with **2e**, **2b**, and IAPP localize in αSyn regions which are well known for their crucial role in αSyn amyloid self-assembly and related cell damage (Figure 5f).[27–28] Their amyloid modulatory functions have been suggested to be mediated by multi-pronged interactions with various parts of αSyn and various other molecules (Figure 5f).[23b,27–28,29] For instance, the N-terminal region αSyn(1–60) is known for its key role in αSyn amyloidogenesis via self-assembly-promoting or -suppressing interactions e.g. with lipids, chaperones, and parts of α(or β)Syn.[22a,28a–f,l,m,30] In this context, intermolecular interactions of αSyn(1–11) or αSyn(1–20) with the C-terminal part αSyn(96–140) of αSyn oligomers or fibrils were found to trigger αSyn amyloidogenesis; by contrast, intramolecular interactions between N- and C-termini of αSyn monomers may protect from aggregation.[28a,b,d,e,m] In addition, αSyn(36–42), known as "P1", has been suggested to be a "master controller" of αSyn amyloid self-assembly while αSyn(45–57), known as "P2" or "pre-NAC" region (αSyn

(45–56)), is an additional key regulator of αSyn amyloid self-assembly.[28f,k] Also, parts of αSyn(34–52) were found to mediate αSyn interactions with diverse amyloid modulators including designed peptides/proteins and small molecules.[8b,c,28g,29b] Finally, MCIP- and IAPP-binding segments αSyn(34–52) and αSyn(87–105) are located in 3 out of 4 recently identified small molecule binding pockets of fαSyn.[28i]

The potent inhibitor function of the MCIPs on both self- and fIAPP cross-seeded αSyn amyloid self-assembly is thus likely mediated by high affinity interactions with αSyn via 3 αSyn segments which localize in regions known for their crucial role in αSyn amyloid self-assembly and were here identified as key sites of its cross-interactions with IAPP as well (Scheme 2). Together with previous results by others, our findings suggest that MCIPs' multi-site binding to αSyn blocks interactions underlying αSyn misfolding cytotoxic di-/oligomerization, (self-)seeding, and fIAPP-mediated mediated cross-seeding and support the suggestion that multi-site targeting of αSyn could be a key requirement for effective anti-amyloid function (Scheme 2).[22a,23b,27–28] Our results also suggest that MCIPs' ability to mimic IAPP sites mediating IAPP/αSyn cross-interactions accounts for multi-site targeting of αSyn and support the notion that common molecular recognition features of Aβ, IAPP, and αSyn exist which can be exploited to develop multi-functional anti-amyloid molecules.[7d,11,23b,29b,32]
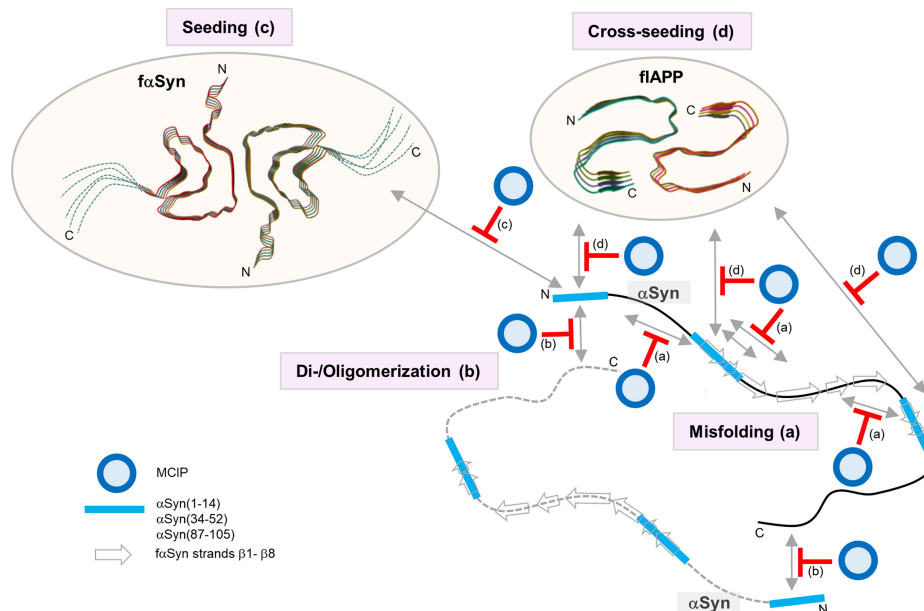


**Scheme 2.** Schematic overview of proposed multi-site targeting mechanism of inhibitory function of MCIPs on both self- and fIAPP-cross-seeded αSyn amyloid self-assembly. High affinity binding of MCIPs (blue circles) to the three identified αSyn key sites blocks crucial interactions of αSyn with αSyn, fαSyn, and (f)IAPP found previously ((a)-(c))[22a,23b,27–28] or in this work (d) to underlie αSyn misfolding (a), di-/oligomerization (b), seeding by fαSyn (c), and cross-seeding by fIAPP (d) (events in pink rectangles). αSyn monomers are shown in intrinsically disordered state; blue bars, identified αSyn key segments; grey arrows, β-strand forming regions in fαSyn fold of Guerrero-Ferreira et al.[27]; the fαSyn model is a modification of the fαSyn fold of Guerrero-Ferreira et al.;[27] the fIAPP model is the fIAPP fold of Roeder et al.[31]

## Conclusions

Here we show that the macrocyclic peptides **2b** and **2e**, designed to mimic IAPP self-/cross-interaction sites and previously found to be potent inhibitors of amyloid self-assembly of IAPP and/or the amyloid-β peptide (Aβ) of Alzheimer's disease (AD), are nanomolar inhibitors of both self- and IAPP-cross-seeded amyloid self-assembly of αSyn. Our results suggest that their anti-amyloid function is mediated by nanomolar affinity interactions with αSyn via three αSyn segments which are identified as key sites of both αSyn self- and its cross-interactions with IAPP. Furthermore, we show that **2b** and **2e** are also able to block Aβ42-mediated cross-seeding of αSyn. Based on their broad spectrum amyloid inhibitor activity and additional drug-like properties, these macrocyclic peptides are promising leads for multifunctional anti-amyloid drugs in PD, T2D, AD, and their comorbidities and studies in animal models are now an important next step. In addition, the identified key αSyn segments shall serve as valuable targets for the design of novel, multi-site targeting molecules as effective anti-amyloids in PD and related synucleinopathies.

## Conflict of Interest

Potential conflict of interest: A. Spanopoulou, L. Heidrich, J. Bernhagen, and A. Kapurniotu are co-inventors of a European Patent Application and an US Patent No. US 11, 498,943 (by TUM) related to the macrocyclic peptides of our manuscript and potential biomedical applications in AD and T2D. In addition, S. Hornung and A. Kapurniotu are co-inventors in a European Patent Application filled by TUM in 2024 related to the peptides of the manuscript and potential biomedical applications in PD, synucleinopathies, and comorbidities. The remaining authors declare no competing interests.

## Data Availability Statement

The data that support the findings of this study are available from the corresponding author upon reasonable request.

**Keywords:** α-synuclein · protein-protein interactions · (cross-)seeding · self-assembly · amyloid inhibitor

[1] a) P. C. Ke, R. Zhou, L. C. Serpell, R. Riek, T. P. J. Knowles, H. A. Lashuel, E. Gazit, I. W. Hamley, T. P. Davis, M. Fandrich, D. E. Otzen, M. R. Chapman, C. M. Dobson, D. S. Eisenberg, R. Mezzenga, *Chem. Soc. Rev.* **2020**, *49*, 5473–5509; b) F. Chiti, C. M. Dobson, *Annu. Rev. Biochem.* **2017**, *86*, 27–68.

[2] a) H. A. Lashuel, C. R. Overk, A. Oueslati, E. Masliah, *Nat. Rev. Neurosci.* **2013**, *14*, 38–48; b) S. Neupane, E. De Cecco, A. Aguzzi, *J. Mol. Biol.* **2023**, *435*, 167930.

[3] P. Westermark, A. Andersson, G. T. Westermark, *Physiol. Rev.* **2011**, *91*, 795–826.

[4] a) D. Athauda, J. Evans, A. Wernick, G. Virdi, M. L. Choi, M. Lawton, N. Vijiaratnam, C. Girges, Y. Ben-Shlomo, K. Ismail, H. Morris, D. Grosset, T. Foltynie, S. Gandhi, *J Mov Disord* **2022**, *37*, 1612–1623; b) C. M. Labandeira, A. Fraga-Bau, D. Arias Ron, E. Alvarez-Rodriguez, P. Vicente-Alba, J. Lago-Garma, A. I. Rodriguez-Perez, *Neural Regen Res* **2022**, *17*, 1652–1658; c) Y. Q. Lv, L. Yuan, Y. Sun, H. W. Dou, J. H. Su, Z. P. Hou, J. Y. Li, W. Li, *Transl Neurodegener* **2022**, *11*, 14.

[5] a) I. Horvath, P. Wittung-Stafshede, *Proc. Natl. Acad. Sci. USA* **2016**, *113*, 12473–12477; b) T. Werner, I. Horvath, P. Wittung-Stafshede, *J Parkinsons Dis* **2020**, *10*, 819–830; c) L. Meng, Y. Li, C. Liu, G. Zhang, J. Chen, M. Xiong, L. Pan, X. Zhang, G. Chen, J. Xiong, C. Liu, X. Xu, L. Bu, Z. Zhang, Z. Zhang, *Prog. Neurobiol.* **2023**, *226*, 102462; d) I. Martinez-Valbuena, I. Amat-Villegas, R. Valenti-Azcarate, M. D. M. Carmona-Abellan, I. Marcilla, M. T. Tunon, M. R. Luquin, *Acta Neuropathol.* **2018**, *135*, 877–886.

[6] a) F. Bassil, H. J. Brown, S. Pattabhiraman, J. E. Iwasyk, C. M. Maghames, E. S. Meymand, T. O. Cox, D. M. Riddle, B. Zhang, J. Q. Trojanowski, V. M. Lee, *Neuron* **2023**, *111*, 3699; b) M. B. Fares, B. Maco, A. Oueslati, E. Rockenstein, N. Ninkina, V. L. Buchman, E. Masliah, H. A. Lashuel, *Proc. Natl. Acad. Sci. USA* **2016**, *113*, E912–921.

[7] a) P. Joshi, M. Vendruscolo, *Adv. Exp. Med. Biol.* **2015**, *870*, 383–400; b) H. Lu, Q. Zhou, J. He, Z. Jiang, C. Peng, R. Tong, J. Shi, *Signal Transduct Target Ther* **2020**, *5*, 213; c) J. A. Wells, C. L. McClendon, *Nature* **2007**, *450*, 1001–1009; d) V. Armien-

to, A. Spanopoulou, A. Kapurniotu, *Angew. Chem. Int. Ed. Engl.* **2020**, *59*, 3372–3384.

[8] a) H. Grosso Jasutkar, S. E. Oh, M. M. Mouradian, *Pharmacol. Rev.* **2022**, *74*, 207–237; b) S. G. Allen, R. M. Meade, L. L. White Stenner, J. M. Mason, *Mol. Neurodegener.* **2023**, *18*, 80; c) S. Pena-Diaz, J. Garcia-Pardo, S. Ventura, *Pharmaceutica* **2023**, *15*.

[9] a) A. A. Vinogradov, Y. Yin, H. Suga, *J. Am. Chem. Soc.* **2019**, *141*, 4167–4181; b) M. Muttenthaler, G. F. King, D. J. Adams, P. F. Alewood, *Nat. Rev. Drug Discovery* **2021**, *20*, 309–325; c) X. Ji, A. L. Nielsen, C. Heinis, *Angew. Chem. Int. Ed. Engl.* **2024**, *63*, e202308251; d) H. Zhang, S. Chen, *RSC Chem Biol* **2022**, *3*, 18–31.

[10] D. Goyal, S. Shuaib, S. Mann, B. Goyal, *ACS Comb. Sci.* **2017**, *19*, 55–80.

[11] A. Spanopoulou, L. Heidrich, H. R. Chen, C. Frost, D. Hrle, E. Malideli, K. Hille, A. Grammatikopoulos, J. Bernhagen, M. Zacharias, G. Rammes, A. Kapurniotu, *Angew. Chem. Int. Ed. Engl.* **2018**, *57*, 14503–14508.

[12] E. Andreetto, E. Malideli, L. M. Yan, M. Kracklauer, K. Farbiarz, M. Tatarek-Nossol, G. Rammes, E. Prade, T. Neumuller, A. Caporale, A. Spanopoulou, M. Bakou, B. Reif, A. Kapurniotu, *Angew. Chem. Int. Ed. Engl.* **2015**, *54*, 13095–13100.

[13] M. Bakou, K. Hille, M. Kracklauer, A. Spanopoulou, C. V. Frost, E. Malideli, L. M. Yan, A. Caporale, M. Zacharias, A. Kapurniotu, *J. Biol. Chem.* **2017**, *292*, 14587–14602.

[14] a) L. M. Yan, A. Velkova, M. Tatarek-Nossol, E. Andreetto, A. Kapurniotu, *Angew. Chem. Int. Ed. Engl.* **2007**, *46*, 1246–1252; b) K. Tas, B. D. Volta, C. Lindner, O. El Bounkari, K. Hille, Y. Tian, X. Puig-Bosch, M. Ballmann, S. Hornung, M. Ortner, S. Prem, L. Meier, G. Rammes, M. Haslbeck, C. Weber, R. T. A. Megens, J. Bernhagen, A. Kapurniotu, *Nat. Commun.* **2022**, *13*, 5004; c) A. Velkova, M. Tatarek-Nossol, E. Andreetto, A. Kapurniotu, *Angew. Chem. Int. Ed. Engl.* **2008**, *47*, 7114–7118; d) L. M. Yan, A. Velkova, M. Tatarek-Nossol, G. Rammes, A. Sibaev, E. Andreetto, M. Kracklauer, M. Bakou, E. Malideli, B. Goke, J. Schirra, M. Storr, A. Kapurniotu, *Angew. Chem. Int. Ed. Engl.* **2013**, *52*, 10378–10383; e) P. Krotee, S. L. Griner, M. R. Sawaya, D. Cascio, J. A. Rodriguez, D. Shi, S. Philipp, K. Murray, L. Saelices, J. Lee, P. Seidler, C. G. Glabe, L. Jiang, T. Gonen, D. S. Eisenberg, *J. Biol. Chem.* **2018**, *293*, 2888–2902.

[15] a) E. Andreetto, L. M. Yan, M. Tatarek-Nossol, A. Velkova, R. Frank, A. Kapurniotu, *Angew. Chem. Int. Ed. Engl.* **2010**, *49*, 3081–3085; b) J. J. Wiltzius, S. A. Sievers, M. R. Sawaya, D. Eisenberg, *Protein Sci.* **2009**, *18*, 1521–1530.

[16] M. R. Eftink, in *Methods in Enzymology: Fluorescence Spectroscopy, Vol. 278* (Eds.: L. Brand, M. L. Johnson), Academic Press, San Diego, **1997**, pp. 221–257.

[17] E. Andreetto, L. M. Yan, A. Caporale, A. Kapurniotu, *ChemBioChem* **2011**, *12*, 1313–1322.

[18] M. Tornquist, T. C. T. Michaels, K. Sanagavarapu, X. Yang, G. Meisl, S. I. A. Cohen, T. P. J. Knowles, S. Linse, *Chem. Commun.* **2018**, *54*, 8667–8684.

[19] L. M. Yan, M. Tatarek-Nossol, A. Velkova, A. Kazantzis, A. Kapurniotu, *Proc. Natl. Acad. Sci. USA* **2006**, *103*, 2046–2051.

[20] Z. Niu, E. Prade, E. Malideli, K. Hille, A. Jussupow, Y. G. Mideksa, L. M. Yan, C. Qian, M. Fleisch, A. C. Messias, R. Sarkar, M. Sattler, D. C. Lamb, M. J. Feige, C. Camilloni, A. Kapurniotu, B. Reif, *Angew. Chem. Int. Ed. Engl.* **2020**, *59*, 5771–5781.

[21] a) S. T. Kumar, S. Donzelli, A. Chiki, M. M. K. Syed, H. A. Lashuel, *J. Neurochem.* **2020**, *153*, 103–119; b) N. Lorenzen, S. B. Nielsen, A. K. Buell, J. D. Kaspersen, P. Arosio, B. S. Vad, W. Paslawski, G. Christiansen, Z. Valnickova-Hansen, M. Andreasen, J. J. Enghild, J. S. Pedersen, C. M. Dobson, T. P.

Knowles, D. E. Otzen, *J. Am. Chem. Soc.* **2014**, *136*, 3859–3868; c) B. Fauvet, M. K. Mbefo, M. B. Fares, C. Desobry, S. Michael, M. T. Ardah, E. Tsika, P. Coune, M. Prudent, N. Lion, D. Eliezer, D. J. Moore, B. Schneider, P. Aebischer, O. M. El-Agnaf, E. Masliah, H. A. Lashuel, *J. Biol. Chem.* **2012**, *287*, 15345–15364.

[22] a) G. Fusco, S. W. Chen, P. T. F. Williamson, R. Cascella, M. Perni, J. A. Jarvis, C. Cecchi, M. Vendruscolo, F. Chiti, N. Cremades, L. Ying, C. M. Dobson, A. De Simone, *Science* **2017**, *358*, 1440–1443; b) R. Cascella, S. W. Chen, A. Bigi, J. D. Camino, C. K. Xu, C. M. Dobson, F. Chiti, N. Cremades, C. Cecchi, *Nat. Commun.* **2021**, *12*, 1814.

[23] a) R. Kayed, E. Head, J. L. Thompson, T. M. McIntire, S. C. Milton, C. W. Cotman, C. G. Glabe, *Science* **2003**, *300*, 486–489; b) M. Chemerovski-Glikman, E. Rozentur-Shkop, M. Richman, A. Grupi, A. Getler, H. Y. Cohen, H. Shaked, C. Wallin, S. K. Warmlander, E. Haas, A. Graslund, J. H. Chill, S. Rahimipour, *Chemistry* **2016**, *22*, 14236–14246.

[24] a) M. J. Diogenes, R. B. Dias, D. M. Rombo, H. Vicente Miranda, F. Maiolino, P. Guerreiro, T. Nasstrom, H. G. Franquelim, L. M. Oliveira, M. A. Castanho, L. Lannfelt, J. Bergstrom, M. Ingelsson, A. Quintas, A. M. Sebastiao, S. V. Lopes, T. F. Outeiro, *J. Neurosci.* **2012**, *32*, 11750–11762; b) F. van Diggelen, D. Hrle, M. Apetri, G. Christiansen, G. Rammes, A. Tepper, D. E. Otzen, *PLoS One* **2019**, *14*, e0213663.

[25] a) M. Hollerhage, J. N. Goebel, A. de Andrade, T. Hildebrandt, A. Dolga, C. Culmsee, W. H. Oertel, B. Hengerer, G. U. Hoglinger, *Neurobiol. Aging* **2014**, *35*, 1700–1711; b) M. Hollerhage, C. Moebius, J. Melms, W. H. Chiu, J. N. Goebel, T. Chakroun, T. Koeglsperger, W. H. Oertel, T. W. Rosler, M. Bickle, G. U. Hoglinger, *Sci. Rep.* **2017**, *7*, 11469.

[26] F. Bassil, H. J. Brown, S. Pattabhiraman, J. E. Iwasyk, C. M. Maghames, E. S. Meymand, T. O. Cox, D. M. Riddle, B. Zhang, J. Q. Trojanowski, V. M. Lee, *Neuron* **2020**, *105*, 260–275 e266.

[27] R. Guerrero-Ferreira, N. M. Taylor, D. Mona, P. Ringler, M. E. Lauer, R. Riek, M. Britschgi, H. Stahlberg, *eLife* **2018**, *7*.

[28] a) S. D. Khare, P. Chinchilla, J. Baum, *Curr. Opin. Struct. Biol.* **2023**, *80*, 102579; b) X. Yang, B. Wang, C. L. Hoop, J. K. Williams, J. Baum, *Proc. Natl. Acad. Sci. USA* **2021**, *118*; c) J. K. Williams, X. Yang, T. B. Atieh, M. P. Olson, S. D. Khare, J. Baum, *J. Mol. Biol.* **2018**, *430*, 2360–2371; d) P. Kumari, D. Ghosh, A. Vanas, Y. Fleischmann, T. Wiegand, G. Jeschke, R. Riek, C. Eichmann, *Proc. Natl. Acad. Sci. USA* **2021**, *118*; e) R. P. McGlinchey, X. Ni, J. A. Shadish, J. Jiang, J. C. Lee, *Proc. Natl. Acad. Sci. USA* **2021**, *118*; f) C. P. A. Doherty, S. M. Ulamec, R. Maya-Martinez, S. C. Good, J. Makepeace, G. N. Khan, P. van Oosten-Hawle, S. E. Radford, D. J. Brockwell, *Nat. Struct. Mol. Biol.* **2020**, *27*, 249–259; g) E. A. Mirecka, H. Shaykhalishahi, A. Gauhar, S. Akgul, J. Lecher, D. Willbold, M. Stoldt, W. Hoyer, *Angew. Chem. Int. Ed. Engl.* **2014**, *53*, 4227–4230; h) E. D. Agerschou, P. Flagmeier, T. Saridaki, C. Galvagnion, D. Komnig, L. Heid, V. Prasad, H. Shaykhalishahi, D. Willbold, C. M. Dobson, A. Voigt, B. Falkenburger, W. Hoyer, A. K. Buell, *eLife* **2019**, *8*; i) Y. Tao, W. Xia, Q. Zhao, H. Xiang, C. Han, S. Zhang, W. Gu, W. Tang, Y. Li, L. Tan, D. Li, C. Liu, *Nat. Chem. Biol.* **2023**, *19*, 1235–1245; j) B. Li, P. Ge, K. A. Murray, P. Sheth, M. Zhang, G. Nair, M. R. Sawaya, W. S. Shin, D. R. Boyer, S. Ye, D. S. Eisenberg, Z. H. Zhou, L. Jiang, *Nat. Commun.* **2018**, *9*, 3609; k) S. M. Ulamec, R. Maya-Martinez, E. J. Byrd, K. M. Dewison, Y. Xu, L. F. Willis, F. Sobott, G. R. Heath, P. van Oosten Hawle, V. L. Buchman, S. E. Radford, D. J. Brockwell, *Nat. Commun.* **2022**, *13*, 4986; l) G. Fusco, A. De Simone, T. Gopinath, V. Vostrikov, M. Vendruscolo, C. M. Dobson, G. Veglia, *Nat. Commun.* **2014**, *5*, 3827; m) B. M. Burmann, J. A. Gerez, I. Matecko-Burmann, S. Campioni, P. Kumari, D.

Ghosh, A. Mazur, E. E. Aspholm, D. Sulskis, M. Wawrzyniuk, T. Bock, A. Schmidt, S. G. D. Rudiger, R. Riek, S. Hiller, *Nature* **2020**, *577*, 127–132.

[29] a) H. Shaykhalishahi, A. Gauhar, M. M. Wordehoff, C. S. Gruning, A. N. Klein, O. Bannach, M. Stoldt, D. Willbold, T. Hard, W. Hoyer, *Angew. Chem. Int. Ed. Engl.* **2015**, *54*, 8837–8840; b) H. Shaykhalishahi, E. A. Mirecka, A. Gauhar, C. S. Gruning, D. Willbold, T. Hard, M. Stoldt, W. Hoyer, *ChemBioChem* **2015**, *16*, 411–414.

[30] E. Cholak, K. Bugge, A. Khondker, K. Gauger, E. Pedraz-Cuesta, M. E. Pedersen, S. Bucciarelli, B. Vestergaard, S. F. Pedersen, M. C. Rheinstadter, A. E. Langkilde, B. B. Krage-lund, *FASEB J.* **2020**, *34*, 7462–7482.

[31] C. Roder, T. Kupreichyk, L. Gremer, L. U. Schafer, K. R. Pothula, R. B. G. Ravelli, D. Willbold, W. Hoyer, G. F. Schroder, *Nat. Struct. Mol. Biol.* **2020**, *27*, 660–667.

[32] A. Frydman-Marom, R. Shaltiel-Karyo, S. Moshe, E. Gazit, *Amyloid* **2011**, *18*, 119–127.